Constant Modulus Waveform Design for Wideband Multicarrier Joint Communications and Sensing via Deep Unfolding

Prashanth Krishnananthalingam, Nhan Thanh Nguyen, Markku Juntti
Centre for Wireless Communications, University of Oulu, P.O.Box 4500, FI-90014, Finland
Emails: {prashanth.krishnananthalingam, nhan.nguyen, markku.juntti}@oulu.fi

2024 IEEE Wireless Communications and Networking Conference (WCNC) | 979-8-3503-0358-2/24/$31.00 ©2024 IEEE | DOI: 10.1109/WCNC57260.2024.10571059

***Abstract*—Joint communications and sensing (JCAS) have recently emerged as a promising technology to utilize the scarce spectrum in wireless networks and to reuse the same hardware to save infrastructure costs. In practical JCAS systems, dual functional constant-modulus waveforms can avoid signal distortion in nonlinear power amplifiers. However, the designs of such waveforms are highly complex due to the nonconvex constant-modulus constraint and high-dimensional variables, especially in wideband multicarrier systems. In this paper, we propose an efficient deep unfolding-based waveform design in a wideband large multiple-input multiple-output (MIMO) JCAS system. The deep unfolding model has a sparsely-connected structure and is trained in an unsupervised fashion. Simulation results show that the proposed deep unfolding design achieves better communications-sensing performance tradeoff while performing 98.5% faster than the conventional branch-and-bound method.**

***Index Terms*—Joint communications and sensing, MIMO-OFDM, deep unfolding, constant-modulus waveform.**

I. Introduction

The growing demand for spectrum resources has spurred the exploration of innovative solutions, such as the integration of radar and communications functionalities. This convergence naturally leads to *joint communications and sensing* (JCAS), which uses a common set of hardware and signal processing techniques to enable simultaneous radar sensing and wireless communications [1]–[3]. Large bandwidth may be available at mmWave frequency bands, providing potential for large communications rate and high resolutions for radar [4], [5].

In monostatic downlink MIMO JCAS, transmit waveforms are typically optimized to balance communications and sensing performances. Conventional techniques, such as manifold optimization [6] and semi-definite relaxation [7], [8], generally yield satisfactory performance but at the cost of high computational complexity and run time. In practical sensing applications, a *constant-modulus* waveform is preferred to avoid signal distortion in non-linear power amplifiers [9]–[12]. However, the design and optimization of such signals are challenging due to the constant modulus, requiring a cumbersome approach such as a branch and bound (BnB) algorithm [9]. To facilitate JCAS designs, deep learning (DL) models, including end-to-end deep auto-encoders [13], [14], deep reinforcement learning [15], and convolutional neural networks [16], have been introduced recently. These models were mainly based on data training. Although they offer computational efficiency and simplify the JCAS designs, they lack interpretability and explainability compared to conventional optimization methods. In contrast, *deep unfolding* is a model-based DL technique relying on both domain knowledge and learning capabilities of DL models [17]. It holds promise for efficient JCAS design and optimization [18]. In [19], an unfolding projected gradient ascent (PGA) method was developed to improve communications–sensing performance tradeoff. In [20], an end-to-end model-based DL approach was introduced for JCAS beamforming and receiving design. However, all these existing model-based DL architectures focused on transceiver designs rather than JCAS constant-modulus waveform designs.

In this paper, we focus on designing constant-modulus waveforms for wideband MIMO orthogonal frequency-division multiplexing (OFDM) JCAS systems. Our approach involves minimizing a weighted sum of multiuser interference (MUI) and the mismatch between the actual transmit waveform and an ideal reference sensing beam subject to the nonconvex constant-modulus constraints. Although the MUI minimization does not always guarantee the rate maximization, we use the criterion, because it is tracktable and provides rate maximization at high signal-to-noise ratios (SNRs). To tackle the design problem, we leverage both the learning capabilities of DL models and model-based optimizers in the deep unfolding approach. Specifically, addressing the minimization problem, we unroll the projected gradient descent (PGD) method and utilize unsupervised training to learn the transformation in each PGD iteration. The developed DL model employs sparse connections and is highly generalized to minimize computational complexity while being able to generate a reliable constant-modulus waveform. Extensive simulations show that our proposed method achieves a far better communications-sensing performance tradeoff than the conventional BnB method [9] with significantly reduced computational and time complexities. Thereby the main novelty of the work is in proposing a low-complexity deep unfolding JCAS solution for the constant modulus waveform design.

II. System Model

We consider a monostatic wide-band MIMO OFDM JCAS system where a base station (BS) equipped with N_{t} antennas simultaneously transmits communications data to N single-antenna communications users and a target at the angle of

979-8-3503-0358-2/24/$31.00 ©2024 IEEE

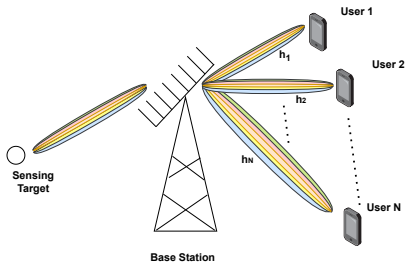

Fig. 1. Multi-carrier joint communications and sensing system.

interest as shown in Fig. 1. Let K denote the number of subcarriers, and let $f_k = f_c + \mathrm{BW}(2k-1-K)/2K$ be the k-th subcarrier, with BW and f_c denoting the system bandwidth and center frequency, respectively. We assume that all the K subcarriers are used for both communications and sensing.

A. Communication Model

Let M be the length of the communications frame. Over each subcarrier, the BS transmits signal matrix $\mathbf{X}[k] = [\mathbf{x}_1[k], \ldots, \mathbf{x}_m[k], \ldots, \mathbf{x}_M[k]] \in \mathbb{C}^{N_t \times M}$, where $\mathbf{x}_m[k] \in \mathbb{C}^{N_t \times 1}$ is the signal vector transmitted at the m-th frame via subcarrier k. The received signals at the users can be given as

$$\mathbf{Y}[k] = \mathbf{H}[k]\mathbf{X}[k] + \mathbf{V}[k], \tag{1}$$

where $\mathbf{H}[k] = [\mathbf{h}_1^T[k], \ldots, \mathbf{h}_N^T[k]] \in \mathbb{C}^{N \times N_t}$ denotes the channel matrix between the BS and N users, with $\mathbf{h}_n[k] \in \mathbb{C}^{N_t \times 1}$ being the channel vector associated with the n-th user. Furthermore, $\mathbf{V}[k] \in \mathbb{C}^{N \times M}$ denotes the noise matrix, with entries following distribution $v_{n,m}[k] \sim \mathcal{CN}(0, N_0), \forall n, m, k$.

We follow the Saleh-Valenzuela channel model and have [19]

$$\mathbf{h}_n[k] = \beta \sum_{c=0}^{N_c-1} \sum_{p=1}^{N_p} \alpha_{c,p} e^{-j2\pi f_k \tau_{c,p}} \mathbf{a}_t(\theta_{c,p}^t, f_k), \tag{2}$$

where N_c and N_p are the numbers of clusters and scattering paths, $\beta = \sqrt{\frac{N_t}{N_c N_p}}$, $\alpha_{c,p}$ and $\tau_{c,p}$ denote the complex gain and the path delay of p-th path in the c-th cluster, respectively. We assume that a uniform linear array is deployed at the BS with half-wavelength spacing. Thus, the array response vector $\mathbf{a}_t$ can be given as $\mathbf{a}_t(\theta_{c,p}^t, f_k) = \frac{1}{\sqrt{N_t}} \left[1, \ldots, e^{j\pi \frac{f_k}{f_c}(N_t-1)\sin\theta_{c,p}^t}\right]^T$, where $\theta_{c,p}^t$ represents the angles of departure (AoD) of the p-th path in the c-th cluster.

Let $\mathbf{S}[k] = [\mathbf{s}_1[k], \ldots, \mathbf{s}_m[k], \ldots, \mathbf{s}_M[k]] \in \mathbb{C}^{N \times M}$ be the desired symbol matrix to be received by the communications users at the k-th subcarrier. Here, $\mathbf{s}_m[k] \in \mathbb{C}^{N \times 1}$ is the desired signal vector intended for the m-th user. We re-express $\mathbf{Y}[k]$ in (1) as

$$\mathbf{Y}[k] = \underbrace{\mathbf{S}[k]}_{\text{symbols}} + \underbrace{(\mathbf{H}[k]\mathbf{X}[k] - \mathbf{S}[k])}_{\text{multiuser interference}} + \underbrace{\mathbf{V}[k]}_{\text{noise}}. \tag{3}$$

The second term in (3) represents the multiuser interference, whose total power over all the subcarriers is given as

$$\gamma(\{\mathbf{X}[k]\}) = \sum_{k=0}^{K-1} \|\mathbf{H}[k]\mathbf{X}[k] - \mathbf{S}[k]\|_{\mathcal{F}}^2, \tag{4}$$

where $\|\cdot\|_{\mathcal{F}}$ denotes the Frobenius norm of a matrix. Based on (3), the average per-subcarrier communications sum rate of the users can be given as [9]

$$R = \frac{1}{K} \sum_{k=1}^{K} \sum_{m=1}^{M} \sum_{n=1}^{N} \log_2 \left(1 + \frac{\mathbb{E}\left\{|s_{n,m}[k]|^2\right\}}{\mathbb{E}\left\{|\mathbf{h}_n[k]^T\mathbf{x}_m[k] - s_{n,m}[k]|^2\right\} + N_0}\right), \tag{5}$$

where $s_{n,m}[k]$ denotes the (*n, m*)-th entry of $\mathbf{S}[k]$.

B. Radar Model

The average sensing beampattern gain for an arbitrary target angle $\theta \in [-90°, 90°]$ can be written as

$$P_d(\theta, f_k) = \frac{1}{KM} \sum_{k=0}^{K-1} \mathbf{a}_t^H(\theta, f_k)\mathbf{X}[k]\mathbf{X}[k]^H\mathbf{a}_t(\theta, f_k). \tag{6}$$

To ensure the sensing performance, the beampattern generated by $\mathbf{X}[k]$ should cover both the sensing target and communications user. Let $\mathbf{X}_0[k] \in \mathbb{C}^{N_t \times M}$ serve as the reference for the radar sensing waveform at the k-th subcarrier. Then, the quality of the waveform generated at the BS can be measured by the mismatch between the overall ideal benchmark waveform and the transmit waveform. Such mismatch is expressed as

$$\zeta(\{\mathbf{X}[k]\}) = \sum_{k=0}^{K-1} \|\mathbf{X}[k] - \mathbf{X}_0[k]\|_{\mathcal{F}}^2. \tag{7}$$

C. Problem Formulation

We are interested in designing the constant-modulus waveform for a good communications-sensing performance trade-off. To this end, we consider minimizing a weighted sum between the multiuser interference and the waveform mismatch in (4) and (7), respectively, subject to constant-modulus constraints. This design is formulated in the problem

$$\underset{\{\mathbf{X}[k]\}}{\text{minimize}} \quad \rho\gamma(\{\mathbf{X}[k]\}) + (1-\rho)\zeta(\{\mathbf{X}[k]\}), \tag{8a}$$

$$\text{subject to} \quad |[\mathbf{X}[k]]_{i,m}| = \sqrt{\frac{P_t}{N_t}}, \ \forall i, m, k. \tag{8b}$$

where ρ is the weighting factor for the communications multiuser interference power, $[\mathbf{X}[k]]_{i,m}$ represents the (i,m)-th entry of $\mathbf{X}[k]$, and $|[\mathbf{X}[k]]_{i,m}|$ is its modulus. Furthermore, P_t denotes the transmit power at each subcarrier and is assumed to be equal for all the subcarriers. Constraint (8b) is non-convex, and the NP-hard nature of the problem results in circular feasible regions of radius $\sqrt{P_t/N_t}$ for $[\mathbf{X}[k]]_{i,m}, \forall i, m$. To overcome the design challenges, we propose the deep unfolding waveform design, elaborated in the next section.

III. Proposed Waveform Design

A. Problem Reformulation

Let $\mathbf{x}_m[k]$, $\mathbf{s}_m[k]$, and $\mathbf{x}_{0m}[k]$ denote the m-th columns of $\mathbf{X}[k]$, $\mathbf{S}[k]$, and $\mathbf{X}_0[k]$, respectively. With these newly introduced notations, the objective function in (8a) and constraint in (8b) can be rewritten as

$$\sum_{k=0}^{K-1}\sum_{m=1}^{M}\rho\left\|\mathbf{H}[k]\mathbf{x}_m[k]-\mathbf{s}_m[k]\right\|^2+(1-\rho)\left\|\mathbf{x}_m[k]-\mathbf{x}_{0m}[k]\right\|^2 \tag{9}$$

and $|x_{i,m,k}|=\sqrt{\frac{P_\mathrm{t}}{N_\mathrm{t}}},\forall i,m,k$, where $x_{i,m,k}$ is the i-th element of $\mathbf{x}_m[k]$, $i=1,\ldots,N_\mathrm{t}$. It is observed that $\{\mathbf{x}_m[k]\}, m=1,\ldots,M, k=1,\ldots,K$ are independent in both the objective function and constraint and thus, can be optimized independently. Based on this observation, we introduce $\mathbf{x}\in\mathbb{C}^{N_\mathrm{t}\times 1}$ and $\mathbf{x}_0\in\mathbb{C}^{N_\mathrm{t}\times 1}$ such that $\mathbf{x}_m[k]=\sqrt{\frac{P_\mathrm{t}}{N_\mathrm{t}}}\mathbf{x}$ and $\mathbf{x}_{0m}[k]=\sqrt{\frac{P_\mathrm{t}}{N_\mathrm{t}}}\mathbf{x}_0$. In other words, we here have dropped the indices (m,k) and normalized the modulus of design variables to unity. As a result, we rewrite problem (8) as

$$\underset{\{\mathbf{X}[k]\}}{\text{minimize}}\quad \rho\left\|\sqrt{\frac{P_\mathrm{t}}{N_\mathrm{t}}}\mathbf{H}\mathbf{x}-\mathbf{s}\right\|^2+(1-\rho)\left\|\sqrt{\frac{P_\mathrm{t}}{N_\mathrm{t}}}(\mathbf{x}-\mathbf{x}_0)\right\|^2, \tag{10a}$$

$$\text{subject to}\quad |x_i|=1,\ \forall i. \tag{10b}$$

where x_i is the i-th element of $\mathbf{x}$, $i=1,\ldots,N_\mathrm{t}$.

B. Structure and Training of Deep Unfolding Model

As in general, machine learning models work with real-valued data, we first introduce the real-valued vectors/matrices $\bar{\mathbf{s}}\in\mathbb{R}^{2N}$, $\bar{\mathbf{x}}\in\mathbb{R}^{2N_\mathrm{t}}$, $\bar{\mathbf{x}}_0\in\mathbb{R}^{2N_\mathrm{t}}$, and $\bar{\mathbf{H}}\in\mathbb{R}^{2N\times 2N_\mathrm{t}}$, which are defined as $\bar{\mathbf{x}}=\begin{bmatrix}\mathrm{Re}(\mathbf{x})\\ \mathrm{Im}(\mathbf{x})\end{bmatrix}$ and

$$\bar{\mathbf{s}}=\begin{bmatrix}\mathrm{Re}(\mathbf{s})\\ \mathrm{Im}(\mathbf{s})\end{bmatrix},\bar{\mathbf{x}}_0=\begin{bmatrix}\mathrm{Re}(\mathbf{x}_0)\\ \mathrm{Im}(\mathbf{x}_0)\end{bmatrix},\bar{\mathbf{H}}=\begin{bmatrix}\mathrm{Re}(\mathbf{H}) & -\mathrm{Im}(\mathbf{H})\\ \mathrm{Im}(\mathbf{H}) & \mathrm{Re}(\mathbf{H})\end{bmatrix}. \tag{11}$$

Then, (10a) has the following equivalent real-valued form

$$f(\bar{\mathbf{x}})=\rho\left\|\sqrt{\frac{P_\mathrm{t}}{N_\mathrm{t}}}\bar{\mathbf{H}}\bar{\mathbf{x}}-\bar{\mathbf{s}}\right\|^2+(1-\rho)\left\|\sqrt{\frac{P_\mathrm{t}}{N_\mathrm{t}}}(\bar{\mathbf{x}}-\bar{\mathbf{x}}_0)\right\|^2. \tag{12}$$

Aiming to minimize $f(\bar{\mathbf{x}})$ with respect to $\bar{\mathbf{x}}$ satisfying (10b), we develop a deep neural network unrolling the iterative PGD optimizer [21]. This technique is typically called deep unfolding. Specifically, let L be the number of layers in the deep unfolding model. Then, the l-th layer is constructed to perform the nonlinear transformation

$$\hat{\mathbf{x}}_l=\prod\left(\hat{\mathbf{x}}_{l-1}-\delta_{l-1}\frac{\partial f(\bar{\mathbf{x}})}{\partial\bar{\mathbf{x}}}\bigg|_{\bar{\mathbf{x}}=\hat{\mathbf{x}}_{l-1}}\right), \tag{13}$$

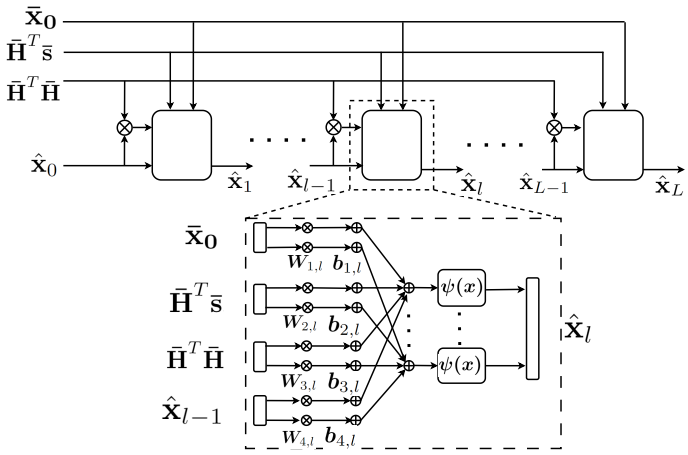

Fig. 2. Architecture of the proposed deep unfolding model.

where $\hat{\mathbf{x}}_l$ and δ_{l-1} denote the solution and the step size in the l-th layer, and $\prod(\cdot)$ is a nonlinear projection operator. Taking the partial derivative in (13), we have

$$\hat{\mathbf{x}}_l=\prod\Bigg(\hat{\mathbf{x}}_{l-1}-\delta_{l-1}\Bigg(2\rho\frac{P_\mathrm{t}}{N_\mathrm{t}}\bar{\mathbf{H}}^T\bar{\mathbf{H}}\hat{\mathbf{x}}_{l-1}-2\rho\sqrt{\frac{P_\mathrm{t}}{N_\mathrm{t}}}\bar{\mathbf{H}}^T\bar{\mathbf{s}}+2(1-\rho)\frac{P_\mathrm{t}}{N_\mathrm{t}}\hat{\mathbf{x}}_{l-1}-2(1-\rho)\frac{P_\mathrm{t}}{N_\mathrm{t}}\bar{\mathbf{x}}_0\Bigg)\Bigg). \tag{14}$$

It is observed that in the l-th layer, $\hat{\mathbf{x}}_l$ is generated based on $\bar{\mathbf{x}}_\mathbf{0}$, $\bar{\mathbf{H}}^T\bar{\mathbf{s}}$, $\bar{\mathbf{H}}^T\bar{\mathbf{H}}$ and $\hat{\mathbf{x}}_{l-1}$. Naturally, these quantities are taken as the inputs of the l-th layer of the deep unfolding model to generate $\hat{\mathbf{x}}_l$, as illustrated in Fig. 2, where $\boldsymbol{W}_{1,l}$, $\boldsymbol{W}_{2,l}$, $\boldsymbol{W}_{3,l}$ and $\boldsymbol{W}_{4,l}$ are the weight matrices, while $\boldsymbol{b}_{1,l}$, $\boldsymbol{b}_{2,l}$, $\boldsymbol{b}_{3,l}$ and $\boldsymbol{b}_{4,l}$ are the bias vectors. For the first layer, $\hat{\mathbf{x}}_0$ can be randomly generated or set to a vector of all zeros [21]. Furthermore, it is important to note that the output vector $\hat{\mathbf{x}}_l$ is constructed by taking the real and imaginary parts of the original vector $\mathbf{x}$ and stacking them as a single column as shown in (11). To ensure appropriate normalization, the elements of $\hat{\mathbf{x}}_l$ are individually normalized. This normalization process involves considering the corresponding real and imaginary parts, calculating the amplitude, and dividing each element by the corresponding amplitude. This meticulous normalization procedure adheres to the constraint in (10b).

Notably, the network exhibits a sparsely connected structure due to the observation that in (14), the i-th element of the left-hand-side only depends on the i-th element of the right-hand-side. In other words, only nodes (or neurons) at the same vertical levels are required to be connected in the deep unfolding network. As a result, $\boldsymbol{W}_{1,l}$, $\boldsymbol{W}_{2,l}$, $\boldsymbol{W}_{3,l}$, and $\boldsymbol{W}_{4,l}$ are diagonal weight matrices. The activation function, denoted as $\boldsymbol{\psi(x)}$, is defined as [22]

$$\psi(x)=-1+2(\sigma(x+0.5)-\sigma(x-0.5)), \tag{15}$$

where $\sigma(\cdot)$ denotes the rectified linear unit (ReLU) function. Here, $\psi(x)\in[-1,1],\forall x$, similar to the tanh activation function, but are nearly-discrete values $\{-1,1\}$ to facilitate constraint (10b). As a result, the output of the l-th layer is

Algorithm 1 Deep Unfolding Multicarrier Waveform Design

for $k = 1 \to K$ **do**
  for $m = 1 \to M$ **do**
    Obtain real input $\bar{\mathbf{H}}, \bar{\mathbf{s}}, \bar{\mathbf{x}}_0$ based on (11) and set $\hat{\mathbf{x}}_0 = \mathbf{0}$.
    for $l = 1 \to L$ **do**
      Output $\hat{\mathbf{x}}_l$ based on (16)–(18) using the set of trained weights and bias $\{\mathbf{W}_{1,l}, \mathbf{W}_{2,l}, \mathbf{W}_{3,l}, \mathbf{W}_{4,l}, \mathbf{b}_l\}$.
      Obtain $\mathbf{x}_m[k]$ by normalizing $\hat{\mathbf{x}}_l$ to ensure (10b).
    end for
  end for
  Set $\mathbf{X}[k] = [\mathbf{x}_1[k], \ldots, \mathbf{x}_M[k]]$
end for

updated as follows:

$$\mathbf{z}_{1,l} = \boldsymbol{W}_{1,l}\bar{\mathbf{x}}_0 + \boldsymbol{b}_{1,l},\ \mathbf{z}_{2,l} = \boldsymbol{W}_{2,l}\bar{\mathbf{H}}^T\bar{\mathbf{s}} + \boldsymbol{b}_{2,l}, \tag{16}$$

$$\mathbf{z}_{3,l} = \boldsymbol{W}_{3,l}\bar{\mathbf{H}}^T\bar{\mathbf{H}}\hat{\mathbf{x}}_{l-1} + \boldsymbol{b}_{3,l}, \mathbf{z}_{4,l} = \boldsymbol{W}_{4,l}\hat{\mathbf{x}}_{l-1} + \boldsymbol{b}_{4,l}, \tag{17}$$

$$\tilde{\mathbf{x}}_l = \mathbf{z}_{1,l} + \mathbf{z}_{2,l} + \mathbf{z}_{3,l} + \mathbf{z}_{4,l},\ \hat{\mathbf{x}}_l = \psi(\tilde{\mathbf{x}}_l). \tag{18}$$

For training, we leverage unsupervised training and employ the following loss function

$$\mathcal{L} = \sum_{l=1}^{L} \rho \left\| \sqrt{\frac{P_{\mathrm{t}}}{N_{\mathrm{t}}}}\bar{\mathbf{H}}\hat{\mathbf{x}}_l - \bar{\mathbf{s}} \right\|^2 + (1-\rho) \left\| \sqrt{\frac{P_{\mathrm{t}}}{N_{\mathrm{t}}}}(\hat{\mathbf{x}}_l - \bar{\mathbf{x}}_0) \right\|^2, \tag{19}$$

which minimizes the objective function based on the outputs of all the L layers in the unfolding model. We note that in the loss function, $\bar{\mathbf{s}}$ and $\bar{\mathbf{x}}_0$ are not the training labels, i.e., they are not feasible solutions to $\mathbf{x}$. In particular, the training does not require any labels.

C. Overall Design and Complexity

We summarize the overall waveform design for problem (8) in Algorithm 1. The algorithm is self-explanatory as the deep unfolding model follows the steps in (16)–(18) to generate the output in each layer. It is noteworthy that the model can generate waveform vectors for multiple users and subcarriers with only one set of trained weights and biases, as an advantage achieved via data training. This lightweight operation significantly contributes to the low complexity and fast execution of the proposed waveform design as it does not require per-subcarrier and per-user processing. Unlike that, in the conventional BnB approach, the branching and bounding are performed for all subcarriers and users.

It can be seen that most of the complexity of the proposed deep unfolding waveform design is to perform the computations in (16)–(18). Note that the weight matrices are all diagonal. Thus, the overall complexity of the proposed design is $\mathcal{O}(KMLN_{\mathrm{t}}^2)$, whereas that of the BnB method increases exponentially with N_{t} [23]. We will further compare the run time of the two schemes in the next section.

IV. Numerical Results

We herein provide numerical results to demonstrate the proposed design. For simulations, we consider a single target at $\theta = 0^\circ$ for all subcarriers. We set $K = 8$, $N_{\mathrm{t}} = 16$, $N = 4$, $M = 20$, and $P_{\mathrm{t}} = 30$ dBm. The channel is generated following the model in Section II-A with $N_{\mathrm{c}} = 5$,

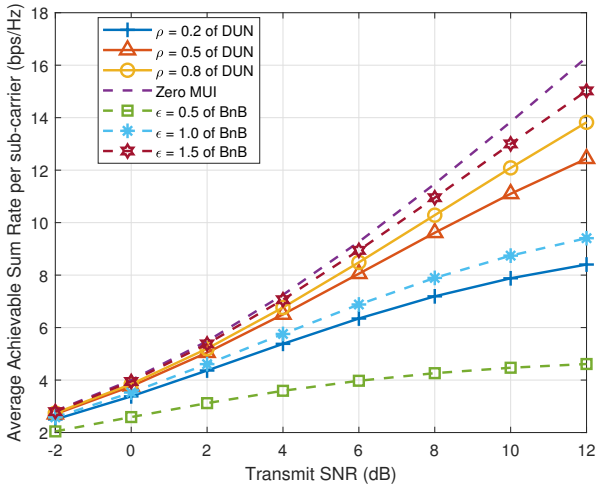

Fig. 3. Average achievable sum rate with SNR for different approaches.

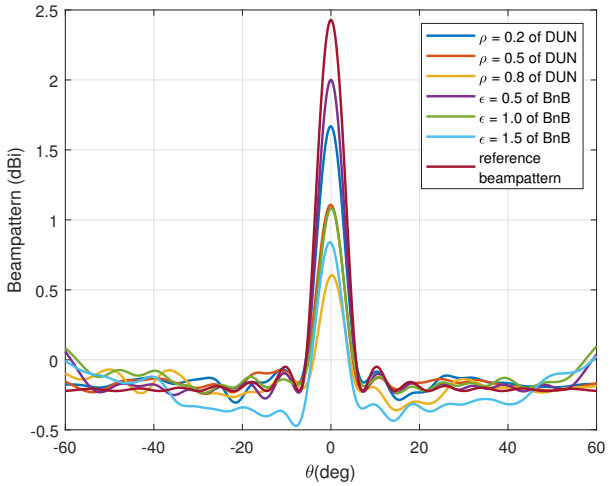

Fig. 4. Average radar beam patterns for different approaches.

$N_{\mathrm{p}} = 10$, $\theta_{c,p}^{\mathrm{t}} \sim U[-\pi/2, \pi/2]$, $\alpha_{c,p} \sim \mathcal{CN}(0,1)$, and $\tau_{c,p} \sim U[0, \tau_{\max}]$, where $\tau_{\max} = QT_{\mathrm{s}}$. Here, $Q = N_{\mathrm{c}}/8$ and $T_s = 1/\mathrm{BW}$ denote the cyclic prefix and symbol period, respectively. The center frequency and bandwidth are set to $f_{\mathrm{c}} = 28$ GHz and $\mathrm{BW} = K\Delta f$, respectively, where $\Delta f = 30.72$ MHz. The desired symbol matrix $\mathbf{S}[k]$ is assumed to be populated with symbols from the unit-power QPSK alphabet. In the simulations, we employ an orthogonal chirp waveform matrix [24] as the radar sensing reference waveform across all subcarriers. The SNR is defined as SNR = P_{t}/N_0. We implement and train the deep unfolding model of $L = 10$ layers with Python and Tensorflow library, using the Adam optimizer, an initial learning rate of 0.0001, and a decaying factor of 0.97.

In Figs. 3, 4 and 5 we compare the per-subcarrier sum rate, beampattern, and the tradeoff between the sum rate and the mean square error (MSE), respectively, of the proposed deep unfolding scheme (referred to as "DUN") to the conventional BnB method. We note that in the BnB scheme, the quality of the waveform $\mathbf{x}$ is ensured via constraint $\|\mathbf{x} - \mathbf{x}_0\|_\infty \leq \epsilon$,

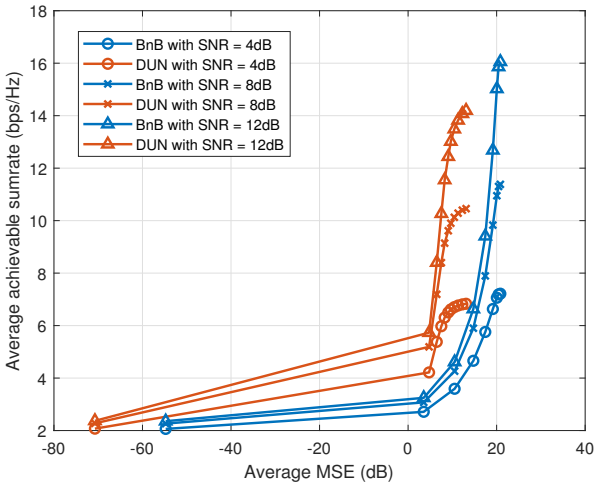

Fig. 5. Average achievable sum rate with average beampattern MSE for different approaches.

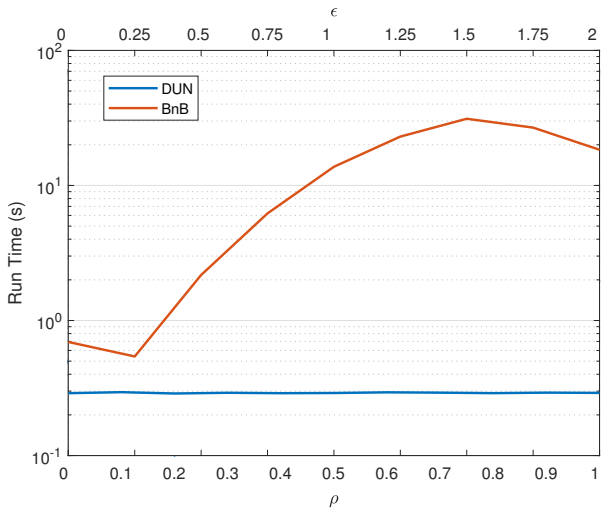

Fig. 6. Average run time for different approaches.

where $\epsilon \in [0, 2]$ [9]. Instead, we have employed the Euclidean distance $\|\mathbf{x} - \mathbf{x}_0\|^2$ and incorporated it into the objective with a weighting factor of $1 - \rho$ as a penalty term to facilitate the unfolding design. There is no specific mapping between ρ and ϵ. Therefore, we show the sum rate and beampatterns of the two for various values of ρ and ϵ in comparison between the two schemes. Due to the constraint and penalty term, it is reasonable to observe in Figs. 3 and 4 that larger ρ and ϵ lead to better communications sum rate but worse sensing beampatterns with lower peaks at the desired target angles $\theta = 0°$.

In Fig. 5, the communications sum rate versus sensing beampattern MSE of the proposed deep unfolding design is obtained for $\rho = \{0, 0.1, \ldots, 1\}$, while those of the conventional BnB approach is attained with $\epsilon = \{0, 0.25, \ldots, 2\}$. More specifically, each marked point on the curves for the deep unfolding and BnB schemes are obtained for each value of ρ and ϵ, respectively. It is seen that for the same SNR, the BnB approach can achieve a slightly larger maximum sum rate than the deep unfolding scheme. However, it has a far worse communications-sensing performance tradeoff than the proposed unfolding design. For example, to achieve the MSE of 10 dB and with SNR $=$ 12 dB, the sum rate offered by the BnB is only 4.5 bps/Hz, which is much lower than 14 bps/Hz attained by the unfolding method. It is also observed that the sum rate of the proposed unfolding method saturates at high MSEs. This happens when ρ becomes sufficiently large in (8a), and thus, the JCAS objective is dominated by the communications metric. In this case, increasing ρ does not lead to significant improvement in the communications sum rate, as seen for high MSEs in Fig. 5.

Finally, we compare the run times of the two schemes. In Table I, we set $N_{\mathrm{t}} = \{8, 16\}$ for the communication-only case, i.e., $\rho = 1$ and $\epsilon = 2$, while $N_{\mathrm{t}} = 16$, $\rho = \{0, 0.1, \ldots, 1\}$, and $\epsilon = \{0, 0.25, \ldots, 2\}$ are considered in Fig. 6 for the deep unfolding and BnB approaches, respectively. It is clear from the table and the figure that the proposed deep unfolding design

Table I. Comparison of the run time of the proposed deep unfolding and BnB methods for $N_{\mathrm{t}} = \{8, 16\}$.

N_{t}	Run time of BnB	Run time of the unfolding scheme
8	17 s	0.277 s
16	18.4 s	0.291 s

performs much faster than the conventional BnB counterpart. Indeed, it has a lightweight structure and does not perform additional per-iteration processing, such as branching and bounding in the BnB method. Furthermore, the average run time required for the waveform design through the proposed unfolding method remains low and almost unchanged with respect to ρ because of the unchanged deep neural network. In contrast, the BnB scheme performs much slower than the unfolding method, especially with average-to-large ϵ.

V. Conclusions

We considered a wideband OFDM-MIMO JCAS system. To ensure the dual communications and sensing functions, we formulated the waveform design problem to minimize the communications multiuser interference and beampattern mismatch. Due to the constant-modulus constraint, the design problem is highly challenging. To overcome the challenge, we developed the deep unfolding model, relying on the PGD approach and data training. Notably, the constructed unfolding model has sparse connections between layers, requiring very low complexity. Our simulation results verified that the proposed unfolding design yields a better communications-sensing performance tradeoff than the conventional BnB scheme, with much lower complexity and run time. In future work, we plan to extend the proposed deep unfolding model to OFDM-MIMO JCAS systems with multiple sensing targets.

Acknowledgement

This research has been supported by the Research Council of Finland through 6G Flagship program under Grant 346208, project DIRECTION under Grant 354901, and Infotech Oulu.

REFERENCES

[1] A. Hassanien, M. G. Amin, E. Aboutanios, and B. Himed, "Dual-function radar communication systems: A solution to the spectrum congestion problem," *IEEE Signal Processing Mag.*, vol. 36, no. 5, pp. 115–126, 2019.

[2] D. Ma, N. Shlezinger, T. Huang, Y. Liu, and Y. C. Eldar, "Joint radar-communication strategies for autonomous vehicles: Combining two key automotive technologies," *IEEE Signal Processing Mag.*, vol. 37, no. 4, pp. 85–97, 2020.

[3] F. Liu, C. Masouros, A. P. Petropulu, H. Griffiths, and L. Hanzo, "Joint radar and communication design: Applications, state-of-the-art, and the road ahead," *IEEE Trans. Commun.*, vol. 68, no. 6, pp. 3834–3862, 2020.

[4] Q. Zhang, X. Wang, Z. Li, and Z. Wei, "Design and performance evaluation of joint sensing and communication integrated system for 5G mmWave enabled CAVs," *IEEE J. Select. Topics Signal Processing*, vol. 15, no. 6, pp. 1500–1514, 2021.

[5] N. T. Nguyen, N. Shlezinger, Y. C. Eldar, and M. Juntti, "Multiuser MIMO wideband joint communications and sensing system with subcarrier allocation," *IEEE Trans. Signal Process.*, 2023.

[6] F. Liu, C. Masouros, A. Li, H. Sun, and L. Hanzo, "MU-MIMO Communications With MIMO Radar: From Co-Existence to Joint Transmission," *IEEE Trans. Wireless Commun.*, vol. 17, no. 4, pp. 2755–2770, 2018.

[7] X. Liu, T. Huang, N. Shlezinger, Y. Liu, J. Zhou, and Y. C. Eldar, "Joint transmit beamforming for multiuser MIMO communications and MIMO radar," *IEEE Trans. Signal Process.*, vol. 68, pp. 3929–3944, 2020.

[8] Y. Ding, S. Yan, X. Zhou, F. Shu, and S. Feng, "Radar-communication waveform design with detection probability constraints," *IEEE Wireless Commun. Lett.*, vol. 12, no. 1, pp. 168–172, 2023.

[9] F. Liu, L. Zhou, C. Masouros, A. Li, W. Luo, and A. Petropulu, "Toward dual-functional radar-communication systems: Optimal waveform design," *IEEE Trans. Signal Process.*, vol. 66, no. 16, pp. 4264–4279, 2018.

[10] B. Tang and P. Stoica, "MIMO multifunction RF systems: Detection performance and waveform design," *IEEE Trans. Signal Process.*, vol. 70, pp. 4381–4394, 2022.

[11] W. Wu, B. Tang, and X. Wang, "Constant-modulus waveform design for dual-function radar-communication systems in the presence of clutter," *IEEE Trans. Aerosp. Electron. Syst.*, 2023.

[12] R. Liu, M. Li, Q. Liu, and A. L. Swindlehurst, "Dual-functional radar-communication waveform design: A symbol-level precoding approach," *IEEE J. Select. Topics Signal Processing*, vol. 15, no. 6, pp. 1316–1331, 2021.

[13] J. M. Mateos-Ramos, J. Song, Y. Wu, C. Häger, M. F. Keskin, V. Yajnanarayana, and H. Wymeersch, "End-to-end learning for integrated sensing and communication," in *Proc. IEEE Int. Conf. Commun.*, Seoul, Republic of Korea, May 2022, pp. 1942–1947.

[14] C. Muth and L. Schmalen, "Autoencoder-based joint communication and sensing of multiple targets," in *Proc. Int. ITG Workshop on Smart Antennas and Conf. on Systems, Commun., and Coding*, Feb. 2023.

[15] L. Xu, R. Zheng, and S. Sun, "A deep reinforcement learning approach for integrated automotive radar sensing and communication," in *Proc. IEEE Sensor Array and Multichannel Sign. Proc. Workshop*, 2022, pp. 316–320.

[16] A. M. Elbir, K. V. Mishra, and S. Chatzinotas, "Terahertz-band joint ultra-massive MIMO radar-communications: Model-based and model-free hybrid beamforming," *IEEE J. Select. Topics Signal Processing*, vol. 15, no. 6, pp. 1468–1483, 2021.

[17] A. Jagannath, J. Jagannath, and T. Melodia, "Redefining wireless communication for 6g: Signal processing meets deep learning with deep unfolding," *IEEE Trans. Artificial Intelligence*, vol. 2, no. 6, pp. 528–536, 2021.

[18] S. Khobahi, N. Shlezinger, M. Soltanalian, and Y. C. Eldar, "LoRD-Net: Unfolded deep detection network with low-resolution receivers," *IEEE Trans. Signal Process.*, vol. 69, pp. 5651–5664, 2021.

[19] N. T. Nguyen, L. V. Nguyen, N. Shlezinger, Y. C. Eldar, A. L. Swindlehurst, and M. Juntti, "Joint communications and sensing hybrid beamforming design via deep unfolding," *arXiv preprint arXiv:2307.04376*, 2023.

[20] J. M. Mateos-Ramos, C. Häger, M. F. Keskin, L. L. Magoarou, and H. Wymeersch, "Model-based end-to-end learning for multi-target integrated sensing and communication," *arXiv preprint arXiv:2307.04111*, 2023.

[21] N. Samuel, T. Diskin, and A. Wiesel, "Learning to detect," *IEEE Trans. Signal Process.*, vol. 67, no. 10, pp. 2554–2564, 2019.

[22] N. Nguyen, M. Ma, N. Shlezinger, Y. C. Eldar, A. Swindlehurst, and M. Juntti, "Deep unfolding-enabled hybrid beamforming design for mmWave massive MIMO systems," in *Proc. IEEE Int. Conf. Acoust., Speech, Signal Processing*, 2023, pp. 1–5.

[23] H. Tuy, *Convex Analysis and Global Optimization*. Berlin, Germany: Springer, 2016.

[24] O. Aldayel, V. Monga, and M. Rangaswamy, "Successive QCQP Refinement for MIMO Radar Waveform Design Under Practical Constraints," *IEEE Trans. Signal Process.*, vol. 64, no. 14, pp. 3760–3774, 2016.